Nonadiabatic dynamics in evaporative cooling of trapped atoms by a radio frequency field

K.-A. Suominen
Helsinki Institute of Physics, PL 9, FIN-00014 Helsingin yliopisto, Finland
Theoretical Physics Division, Department of Physics, University of Helsinki, PL 9, FIN-00014 Helsingin yliopisto, Finland

E. Tiesinga* and P. S. Julienne
Atomic Physics Division, National Institute of Standards and Technology, Gaithersburg, MD 20899-0001
(February 2, 2008)

Magnetically trapped neutral atoms can be cooled with the evaporation technique. This is typically done by using a radiofrequency (rf) field that adiabatically couples trapped and untrapped internal atomic states for atoms with kinetic energies above a value set by the field frequency. The rf-field can also induce nonadiabatic changes of internal atomic spin states (F, M) that lead to heating and enhanced loss of atoms. In this paper we use wave packet simulations to show that the evaporation process can induce these nonadiabatic transitions which change the internal spin state of doubly spin-polarized (2,2) trapped atoms. We also verify the validity of a multistate Landau-Zener model in describing the nonadiabatic dynamics. In addition, we calculate exchange relaxation rate coefficients for collisions between atoms in the $(2, M)$ states of ^{23}Na atoms. Large exchange relaxation coefficients for ^{23}Na as compared to ^{87}Rb $F = 2$ suggest that evaporative cooling of (2,2) Na will be more difficult than for the corresponding state of Rb.

34.90.+q, 32.80.Pj, 42.50.Vk

I. INTRODUCTION

Bose-Einstein condensation has been observed recently in alkali gases [1–4]. This has led to a series of fascinating experiments involving collective excitations [5–9] and atom lasers [10,11]. These experiments take place at very low temperatures, ranging from microkelvins to nanokelvins. Such temperatures can be reached only with evaporative cooling if sufficient atomic densities for condensation are to be obtained. The idea for evaporative cooling was originally developed in connection with attempts to observe Bose-Einstein condensation in spin-polarized hydrogen [12,13] (for a review see Ref. [14]). Although the process has been studied in detail both theoretically and experimentally, some aspects still require clarification.

The basic idea for evaporative cooling is simple. The atoms in a hyperfine state (F, M) are trapped by spatially inhomogeneous magnetic fields. The edges of the trap are then lowered, allowing the hot atoms to escape. Atoms left in the trap collide elastically and eventually a thermal equilibrium is reached, but at some temperature which is lower than the original one. In practice the trap edges are "lowered" by coupling different magnetic substates (spin states) of the atoms with a radiofrequency (rf) field of variable frequency [14,15], as shown in Fig. 1. Within the rotating wave approximation we can shift the energy states by multiples of the radiofrequency field photon energy, and eventually we obtain the curve crossing situation for $F = 2$ featured in Fig. 2 [14]. We can view the evaporation as adiabatic following of the lowest rf-dressed state by the moving atoms. Here we will consider the doubly spin-polarized level $(2, 2)$, for which Bose-Einstein condensation has been achieved for ^{87}Rb but not for ^{23}Na.

The evaporation process requires elastic binary collisions for the rethermalisation of the atoms that remain trapped. However, inelastic collisions can give the collision products large kinetic energies which lead to loss or heating of trapped atoms. The normal mechanism for collisional relaxation of the trapped (2,2) doubly spin-polarized state of ^{87}Rb or ^{23}Na, spin-dipolar relaxation, has a very small collisional rate coefficient [16–18] which would limit the lifetime of a Bose-Einstein condensate to a very acceptable 30 seconds. However, if the evaporation process results in the formation of $(2, 1)$ and $(2, 0)$ spin components via rf-induced nonadiabatic transitions due to atomic motion in the spatially inhomogeneous magnetic field, inelastic collisions between these components and/or the remaining (2,2) spin state can occur by a strong spin-exchange mechanism and in principle lead to large collisional relaxation rates.

The actual size of the relaxation rate is strongly species dependent. In Refs. [19,20] it has been shown that spin relaxation for the collision between (2,2) and $(1, -1)$ for ^{87}Rb is strongly reduced compared with the equivalent collision in ^{23}Na. The rate coefficients are anomalously small for ^{87}Rb, because of the fortuitous near equality of the scattering lengths for the $^3\Sigma_u^+$ and $^1\Sigma_g^+$ states that correlate with the separated ground state atoms. We will also

find in this paper that the various spin-exchange collisional rate coefficients between ^{23}Na $(2, M)$ spin components are about three orders of magnitude larger than the corresponding values for ^{87}Rb.

In this paper we consider two distinct aspects of the relevant physics: (1) the rf-induced nonadiabatic dynamics due to motion in the spatially inhomogeneous magnetic field that move atoms from the primary trapped state (2,2) to the other states of the same hyperfine manifold, and (2) the rate coefficients for collisions involving other $(2, M)$ states. For the first aspect, we consider the coupled five-state multicrossing situation that occurs in the rf-dressed picture for ^{23}Na $(2, M)$ shown in Fig. 2. Especially in the early stages of cooling, when the frequency of the rf-field is large and the crossing between the $(2, M)$ states occurs at very large energies, it is possible that the atoms will not adiabatically follow the rf-dressed potential a shown in Fig. 2. Atoms can, after traversing the crossing, either remain on the bare (2,2) state [21] or move, for example, to the bare (2,1) state. In other words, we have nonadiabatic dynamical transfer between the rf-dressed states. These two bare states are trapping states, so atoms will return to the crossing region instead of escaping from the trap. When they traverse the crossing again, population can move to the spin states (2,1) and (2,0), and then approach the trap center, thus leading to the loss-inducing collisions to be considered as the second aspect of the physics.

The adiabatic following, leading to evaporation, and the unwanted nonadiabatic transitions can be studied by describing atoms with multicomponent wave packets that evolve under a time-dependent Schrödinger equation. This model does not contain all aspects of atomic dynamics during evaporation such as the rethermalization, but does demonstrate adequately the possibility of nonadiabatic transitions and the prospects for harmful inelastic atomic collisions in the trap. It has been proposed that a Landau-Zener model can be used for a semiclassical study of the evaporation as well [14] and we will show that a multistate version of the Landau-Zener model [22–24] describes our wave packet dynamics rather well. This allows one to extrapolate some of our results into a much larger parameter space than we have covered with our wave packet analysis.

The lowest rf-dressed state has nonnegligible contributions from all $(2, M)$ bare states of the $F = 2$ manifold. This is called rf-mixing of the spin states. One might think that the collisions between these mixed states can effectively lead to collisions between the different M-states, especially when the energy difference between the states becomes nonnegligible compared to the strength of the rf-coupling. However, we find that this mixing will not lead to enhanced inelastic collision rates at all. This conclusion agrees with that obtained by Moerdijk *et al.* [25]. The physical reason for this behavior is that the rf-field only rotates the quantization axis, and the T-matrix elements for the inelastic processes change accordingly, not picking up any exchange collision amplitude. Thus the rf-dressed state which has the lowest energy simply obtains the label (2,2) along the new quantization axis. In short, when two atoms in the lowest rf-dressed state collide, the process is equal to a collision between two atoms in the bare (2,2) state.

In this paper we first present the collisional rate coefficients for ^{23}Na $F = 2$ trapping in Sec. II and discuss the rf-mixing of states. Then we demonstrate the nonadiabatic dynamical transfer processes in Sec. III using wave packets. Furthermore, we discuss the multistate Landau-Zener modelling of the dynamics of the evaporation process. Finally, the discussion in Sec. IV concludes the paper.

II. COLLISIONAL LOSS RATES

A. Exchange relaxation rates

The ^{23}Na and ^{87}Rb ground state atoms have two hyperfine components, $F = 1$ and $F = 2$ as shown for ^{23}Na in Fig. 1. The $F = 1$ level is 3-fold degenerate, with components $M = 1, 0, -1$ and the $F = 2$ level is 5-fold degenerate, with components $M = -2, -1, 0, 1, 2$. For magnetic fields below ~ 1 mT the internal energy of the magnetic sublevels depends linearly on the trapping field where the magnetic sublevels are defined with respect to the direction of this field. The F label is strictly speaking only valid for zero magnetic field. However, we wish to determine the inelastic collision rate coefficients in a weak (mT) magnetic field and it turns out that the dominant loss processes are nearly independent of field strength B and are well approximated by the corresponding zero-field rate. We will present $B = 0$ rates and scattering T-matrix elements labeled according to the zero-field labels (F, M) only, but have confirmed numerically that small magnetic fields do not change the rate by more than 20 %.

The (2,2) trapping state is known to relax with a small rate coefficient, on the order of 10^{-15} cm^3/s, due to the weak spin-dipole mechanism [17,18,26]. Relaxation leads to formation of a lower $(1, M)$ state accompanied by the release of a large amount of energy. However, if other $(2, M)$ components of $F = 2$ are present due to rf-induced nonadiabatic motion in the trapping potential, these components may decay via the exchange mechanism. We will show that this mechanism leads to very large rate coefficients for ^{23}Na, greater than 10^{-11} cm^3/s, that is, orders of magnitude larger than for dipolar relaxation. On the other hand, $(2, M)$ components of ^{87}Rb have very small exchange relaxation rate coefficients, on the order of 10^{-14} cm^3/s, just as is known to be the case for exchange collisions between a $(2, 2)$ and

$(1,-1)$ atom [19,20]. The small rate coefficients for ^{87}Rb ensure that this process is not significant for the $F=2$ level of ^{87}Rb, which can be evaporatively cooled and Bose-condensed in the $(2,2)$ state [27]. So far no one has achieved Bose-Einstein condensation for the $(2,2)$ level of ^{23}Na.

We now extend the calculations of Ref. [20] to apply to collisions of two $(2,M)$ atoms as well. We assume that the collision starts with the two atoms in the hyperfine levels (F_1,M_1), (F_2,M_2) and with relative angular momentum state ℓ,m and ends with the atoms in the levels (F_3,M_3), (F_4,M_4) and relative angular momentum state ℓ',m'. At sufficiently low temperature only s-waves contribute, for which $\ell=0$, $m=0$. We introduce symmetrized states of atom pairs that are symmetric with respect to exchange of identical atoms, with half-integer nuclear spin quantum number, and define a symmetrized T-matrix as done by Stoof *et al.* [26] for transitions between the symmetrized states

$$|\{F_iM_i,F_jM_j\}\ell m\rangle=\frac{|F_iM_i,F_jM_j,\ell m\rangle+(-1)^\ell|F_jM_j,F_iM_i,\ell m\rangle}{\sqrt{2(1+\delta_{ij})}}, \tag{1}$$

where $\delta_{ij}=1$ if $F_i=F_j, M_i=M_j$ and $\delta_{ij}=0$ otherwise.

Alternatively this basis is rewritten by noting that the total angular momentum, $\vec{F}_t=\vec{F}_1+\vec{F}_2+\vec{l}=\vec{f}+\vec{l}$, is conserved for $B=0$. Therefore, after vector coupling the $|F_1M_1\rangle$ and $|F_2M_2\rangle$ levels to the resultant symmetrized angular momentum $|F_1F_2f,M_1+M_2\rangle$ states, then vector coupling to the relative angular momentum $|\ell,m\rangle$ to get the total angular momentum states $|F_1F_2f,\ell,F_t,M_t=M_1+M_2+m\rangle$, the symmetrized T-matrix elements are given in terms of the indices $\{F_1F_2f\ell F_t\}$ and are independent of projection quantum numbers M_1,M_2,m,M_t. The T-matrix elements for the symmetrized states of Eq. (1) are given in terms of these T-matrix elements in the total angular momentum basis as [28–30]

$$\begin{aligned}&\langle\{F_3M_3,F_4M_4\}\ell'm'|T|\{F_1M_1,F_2M_2\}\ell m\rangle=\\&\left(\frac{1+\delta_{F_1F_2}}{1+\delta_{F_1F_2}\delta_{M_1M_2}}\right)^{\frac{1}{2}}\left(\frac{1+\delta_{F_3F_4}}{1+\delta_{F_3F_4}\delta_{M_3M_4}}\right)^{\frac{1}{2}}\sum_{ff'F_t}(F_3F_4f'|M_3M_4,M_3+M_4)(f'\ell'F_t|M_3+M_4,m',M_t)\\&\times(F_1F_2f|M_1M_2,M_1+M_2)(f\ell F_t|M_1+M_2,m,M_t)T^{(F_t)}(F_3F_4f'\ell'\leftarrow F_1F_2f\ell),\end{aligned} \tag{2}$$

where $(\ |\ )$ are the Clebsch-Gordan coefficients. We define our T-matrix to be related to the unitary S-matrix by $\mathbf{T}=\mathbf{1}-\mathbf{S}$.

Spin-exchange collisions are only possible if the following selection rules are obeyed: $\ell=\ell'$, $m=m'$, $f=f'$, and $M_1+M_2=M_3+M_4$. Equation (2) simplifies considerably for s-wave collisions, since $\ell=0$ and $f'=f=F_t$; in particular, for s-wave $(2,M_1)+(2,M_2)$ collisions inelastic exchange transitions are only possible if $f=F_t=0$ or 2.

The spin-exchange selection rules show that a doubly-polarized gas cannot decay via this mechanism. However, if the evaporation process produces the other trappable $F=2$ states this is no longer valid. Table I therefore gives explicit formulas that can be used for evaluating the T-matrix amplitudes for $(2,2)+(2,0)$ and $(2,1)+(2,1)$ s-wave exchange collisions. The shorthand notation used in Table I is

$$T^{(2)}_{21}=T^{(2)}(212s\leftarrow 222s), \tag{3}$$

$$T^{(2)}_{11}=T^{(2)}(112s\leftarrow 222s), \tag{4}$$

where the notation means $T^{(F_t)}_{F_3F_4}$. Amplitudes for other $(2,M_1)+(2,M_2)$ s-wave collisions can be worked out using Eq. (2) and the additional matrix element,

$$T^{(0)}_{11}=T^{(0)}(110s\leftarrow 220s). \tag{5}$$

One might expect that $(2,2)+(2,1)$ inelastic exchange collisions will be important. However, since then $M_3+M_4=M_1+M_2=3$, it follows that spin-exchange matrix elements with $f=f'=3$ or 4 contribute. For s-wave scattering there is only one spin state with either value of f. Hence only elastic s-wave T-matrix elements exist while inelastic s-wave spin-exchange transitions are absent. The only remaining $(2,2)+(2,1)$ relaxation mechanism is via the weak dipolar interaction. On the other hand a p-wave exchange relaxation is permitted for $(2,2)+(2,1)$ collisions, where the inelastic $T^{(F_t)}(213p\leftarrow 223p)$ matrix elements contribute as the temperature increases. These T-matrix elements vary as $k^{3/2}$, where $\hbar k$ is the relative momentum, whereas the s-wave amplitudes vary as $k^{1/2}$. In numerical calculations, we find p-wave inelastic exchange collisions will have rate coefficients two orders of magnitude or more smaller than s-wave exchange collisions for temperatures below 10 μK for ^{23}Na collisions. The p-wave contributions rapidly increase with collision energy, and become comparable to the s-wave contributions above 100 μK. Thus, some collisional relaxation

$\{F_3M_3, F_4M_4\} \leftarrow \{2M_1, 2M_2\}$	$\langle\{F_3M_3, F_4M_4\}s\|T\|\{2M_1, 2M_2\}s\rangle$,
$21, 11 \leftarrow 22, 20$	$-\sqrt{2}\sqrt{\frac{2}{21}}T_{21}^{(2)}$
$11, 11 \leftarrow 22, 20$	$\sqrt{2}\sqrt{\frac{2}{7}}T_{11}^{(2)}$
$22, 10 \leftarrow 22, 20$	$\sqrt{2}\frac{2}{\sqrt{21}}T_{21}^{(2)}$
$21, 11 \leftarrow 21, 21$	$\sqrt{\frac{1}{7}}T_{21}^{(2)}$
$11, 11 \leftarrow 21, 21$	$-\sqrt{\frac{3}{7}}T_{11}^{(2)}$
$22, 10 \leftarrow 21, 21$	$-\sqrt{\frac{2}{7}}T_{21}^{(2)}$

TABLE I. Bare exchange scattering T-matrix elements for s-waves

due to $(2,2)+(2,1)$ collisions may be important at the start of evaporation, but such collisions become less significant as the condensation limit is approached.

In order to calculate the actual zero-field exchange collision rates for collisions of ^{23}Na $(2, M)$ levels, we use the same quantum scattering method and model of the ^{23}Na potentials as in Ref. [31]. We adjusted the potentials slightly to locate correctly the positions of the triplet Feshbach resonance levels reported recently [32]; the calculated scattering length for $(1,-1)$ elastic collisions is 52 a_0, in agreement with our previously reported value [31]. We find as $k \to 0$,

$$T_{21}^{(2)} = 5.5e^{-3.1i}\sqrt{k}, \tag{6}$$

$$T_{11}^{(2)} = 3.9e^{-1.4i}\sqrt{k}, \tag{7}$$

$$T_{11}^{(0)} = 6.5e^{-1.6i}\sqrt{k}, \tag{8}$$

where k is expressed in units of a_0^{-1} ($a_0 = 0.0529177$ nm is the Bohr radius of the hydrogen atom). We define $|T_{ij}^{(f)}|^2 = A_{ij}^{(f)}k$ and have $A_{21}^{(2)} = 31$ a_0, $A_{11}^{(2)} = 15$ a_0, and $A_{11}^{(0)} = 43$ a_0. On the other hand, the squared T-matrix for inelastic spin-exchange p-wave scattering is proportional to k^3. In particular, $|T^{(3)}(213p \leftarrow 223p)|^2 = A_{21}^{(3)}k = (2.6 \times 10^5 k^2)k$. This corresponds to $A_{21}^{(3)} = 0.3$ a_0 at 10 μK which as noted is small compared to inelastic s-wave contributions at this collision energy.

The event rate coefficient due to any atom loss process at a relative collision momentum $\hbar k$, using the definition $|T|^2 = Ak$, is conveniently written as

$$K_{\text{event}} = \frac{\pi v}{k^2}|T|^2 = \frac{\pi\hbar}{\mu}A = 1.056 \times 10^{-11}\frac{A(a_0)}{\mu(\text{amu})}\ \frac{\text{cm}^3}{\text{s}} \tag{9}$$

for a Maxwellian gas and half of this for a Bose-Einstein condensate [16]. The quantity μ is the reduced mass and the number of hot atoms produced per event in either case is two, since the released energy is shared equally between the two atoms.

Using Eqs. (6), (8) and Table I, the A coefficients in Eq. (9) for the total event rate of spin-exchange collisions for $(2,2)+(2,0)$ and $(2,1)+(2,1)$ are $\frac{3}{7}(A_{21}^{(2)} + A_{11}^{(2)}) = 20$ a_0 and $\frac{2}{7}(2A_{21}^{(2)} + A_{11}^{(2)}) = 22$ a_0, respectively. The event rate coefficients for these collisions are on the order of 2×10^{-11} cm^3/s for Na. The rate coefficients are in excellent agreement with those calculated numerically for weak magnetic fields in the range 0 mT to 20 mT.

The corresponding inelastic collision strengths A for ^{87}Rb are $A_{21}^{(2)} = 0.064$ a_0, $A_{11}^{(2)} = 0.37$ a_0, and $A_{11}^{(0)} = 0.16$ a_0 for s-waves and $A_{21}^{(3)} = 3.7 \times 10^4 k^2$ for p-waves. These values are obtained as in Ref. [20] with ground state potentials that give scattering lengths of 103 a_0 for both the $(2,2)+(2,2)$ and $(1,-1)+(1,-1)$ collision. The s-wave event rate coefficients are on the order of a few times 10^{-14} cm^3/s, consistent with the small exchange collision rate coefficient of comparable magnitude for ^{87}Rb $(2,2)+(1,-1)$ collisions [19,20,27,33]. The ^{87}Rb exchange collision rate coefficients show stronger sensitivity to weak magnetic field than the ^{23}Na ones [20].

For Bose-Einstein condensation studies the typical atomic densities are on the order of 10^{14} atoms/cm^3. Therefore the three orders of magnitude difference between ^{23}Na and ^{87}Rb rate coefficients implies that even relatively small population transfer from the (2,2) trapped level to the $(2,1)$ and $(2,0)$ states during the evaporation process can cause a strong/unwanted increase in trap loss for ^{23}Na, but has an insignificant effect for ^{87}Rb.

B. Effect of the rf-field on exchange relaxation

The rate coefficients in Sec. II A are evaluated using so-called bare atomic states where the rf-field has not been included. We now turn our attention to the effect of rf-induced dressing on the inelastic collision rate coefficients. The dressing mixes different $(2, M)$ levels and there is a question as to whether this mixing affects the exchange relaxation rates of the dominant (2,2) trapped level. Moerdijk *et al.* [25] have argued that field-dressing has a negligible effect on collisional relaxation. We now discuss the rf-mixing and its consequences.

In a magnetic trap the atoms are held in a position dependent trapping field $\vec{B}_{\rm trap}$. In fact, for a spherically harmonic trapping potential $|\vec{B}_{\rm trap}(\vec{x}) - \vec{B}_{\rm trap}(\vec{0})| \propto x^2$, where $\vec{x} = \vec{0}$ is the center of the trap. This magnetic field defines a space-fixed z-axis at each point in the trap along which the atomic (F, M) states are defined. The variations of the magnetic field strength over the atom cloud are small compared to the field strength in the middle of the trap. Hence if only this trapping field is present the zero-field T-matrix elements and the corresponding rate coefficients are valid everywhere in the trap.

The components of an rf-field, with frequency ν, parallel and perpendicular to the trapping field have different effects on the mixing of states [34]. The latter leads to $|\Delta M| = 1$ transitions. In fact, for the evaporation process the rf-photon energy $h\nu$ is chosen to be nearly resonant with the $(2, 2)$ to $(2, 1)$ transition and since the trapping field is sufficiently weak that the internal energy of the atomic states depends linearly on the field strength the photon is resonant with all adjacent M states as well. The parallel component of the rf-field leads to $|\Delta M| = 0$ transitions. However, the rf-photon is not resonant with the allowed parallel transitions $(1, M) \rightarrow (2, M)$. Therefore, at each point in the trap only the component of the rf-field that is locally perpendicular to the trapping field leads to mixing of atomic sublevels. The amplitude of the rf-field is small compared to the trapping field.

In order to keep the modelling tractable we make several although not crucial simplifications. Variations in the direction of the trapping field over the atom cloud can be neglected. This allows us to use a single z-axis that describes the quantization axis everywhere in the trap. Moreover, the atom-field interaction will be treated using the rotating wave approximation. Then it is convenient to use a coordinate system that rotates with frequency ν around the z-axis. The rf-field is stationary in this coordinate system and is chosen to lie along the rotating x'-axis with a field strength $B_{\rm rf}$. Following Ref. [34] the $F = 2$ atomic hyperfine Hamiltonian coupling to the rf-field can then be interpreted in terms of a magnetic moment $\vec{F}$ rotating around an effective field and we arrive at a local Hamiltonian which describes the motion of the magnetic moment at each position $\vec{x}$ in the magnetic trap

$$H(\vec{x}) = \hbar\sigma(\vec{x})\hat{F}_z + \hbar\Omega\hat{F}_{x'}, \tag{10}$$

where $\hbar\sigma$ is the local energy spacing of the atomic magnetic sublevels, shown as the dotted lines of Fig. 2, and Ω is the zero-detuning Rabi frequency of the atom-field coupling. Here $\hat{F}_z$ and $\hat{F}_{x'}$ are the components of spin-F operators along the z- and x'-axis respectively. Note that for example in the space-fixed x direction it follows

$$\hbar\sigma = \frac{1}{F}\left(\frac{1}{2}m\omega^2x^2 - E_d\right), \tag{11}$$

with $x = 0$ as the trap center, m is the atomic mass and ω is the trap frequency in the x direction. Here E_d is the bare state trap depth (see Fig. 2), defined as the difference between the bare level spacing of adjacent M states in the center of the trap and the rf frequency $h\nu$.

We have assumed for simplicity that the trapping in three dimensions is achieved by a static field [2], and not a TOP trap [1]. In a TOP trap there is an additional fast-oscillating field which has an amplitude comparable to the trapping field. The amplitude of the rf-field used for evaporation is small compared to the trapping field (even at the center of the trap where the trapping field is weakest), which allows the description we presented above. If we simply assume that the fast-oscillating TOP field can be adiabatically eliminated, i.e., we obtain the time-averaged trapping potential, our studies apply also to the TOP trap. The validity of this adiabatic elimination of the TOP field in the presence of the evaporation rf-field is to some extent an open question [35]. It does not fall within the scope of this paper, however, so we do not discuss it further.

A collision between two atoms occurs locally in sub-nanosecond time scales. It is sufficiently fast that the rf-field as seen by the atoms during a collision is frozen [25] (the period of the rf-field is on the order of about 100 ns). Thus the rotating x'-axis can be considered fixed during the collision. Therefore, Eqs. (2)-(9) are again valid but now with spin states $|FM\rangle$ defined relative to a rotating z'-axis. To see this just note that the simple spin structure of Eq. (10) allows us to introduce a transformation R that rotates the z-axis into a z'-axis with the property that the transformed Hamiltonian is of the form $\Delta(\vec{x})F_{z'}$. In fact, it can be shown that this is achieved with a rotation by an angle θ around the axis perpendicular to both z- and x'-axis, where

$$\tan(\theta) = -\frac{\Omega}{\sigma} \tag{12}$$

and $\Delta(\vec{x}) = \hbar\sqrt{\sigma(\vec{x})^2 + \Omega^2}$. The explicit form of the rotation is

$$|FM\rangle_{z'} = \sum_{M'} d^{(F)}_{MM'}(-\theta)|FM'\rangle_z, \tag{13}$$

where the $d^{(F)}_{MM'}$ are rotation matrices [36] and the subscripts z and z' denote the axis along which the state $|FM\rangle$ is defined. Again this z'-axis can be considered fixed during a collision. Consequently, if the atoms before the collision are in an eigenstate of the Hamiltonian (10), the decay processes due to collisions are simply given with the bare rate constants. For example, if the atoms are everywhere in the local doubly-polarized state $|FM\rangle_{z'}$, only the weak spin dipole interaction causes decay of the sample. We have explicitly verified e.g. for the dressed (2,2) state that the exchange transition contributions from the bare states such as (2,1) and (2,0) cancel out completely.

The premise that the atoms are always in the eigenstates of the Hamiltonian (10) hinges on the assumption that the motion of the atoms has a negligible effect. In fact the premise is not always satisfied and Sec. III is devoted to the nonadiabatic effects induced by the motion of a single atom through a spatially varying magnetic field and hence a varying σ. In such a field at each point in the trap the coordinate system with the quantization axis z' is different. This is most inconvenient if we want to follow the motion of a single atom. Therefore, we use the basis of eigenstates $|FM\rangle_z$ of the Hamiltonian (10) when $\Omega = 0$ everywhere in the trap; these are the base states [21]. Of course, for non-zero Ω the Hamiltonian is not diagonal in this basis. There is coupling of adjacent magnetic levels with

$$H_{M,M+1} = H_{M+1,M} = \sqrt{(F-M)(F+M+1)}\hbar\Omega/2. \tag{14}$$

III. DYNAMICS OF EVAPORATION AND NONADIABATIC TRANSITIONS

The calculation of the transition amplitudes in Sec. II shows that for ^{23}Na the collisions between the atoms in an rf-field does not necessarily lead to enhanced inelastic rate coefficients. However, if we consider moving atoms in the absence of collisions, then for an atom initially in the (dressed) doubly polarized spin state it is possible to have nonadiabatic transitions to those rf-dressed states that have strong inelastic processes when they collide with other atoms. As an atom moves fast enough in the spatially inhomogeneous magnetic field, its spin $\vec{F}$ can not follow adiabatically the changing magnetic field. The breakdown of the adiabatic following is especially likely when the rf-field brings the bare states into resonance. Any atom that has enough energy to leave the trap during evaporative cooling will necessarily traverse such a resonance point.

We model the evaporation process by describing the atom as a wave packet. This description takes into account any nonadiabatic process due to the atomic motion as the wave packet moves back and forth in the trap. In other words, we use the time-dependent Schrödinger equation

$$i\hbar\frac{\partial\Psi(\vec{x},t)}{\partial t} = \mathcal{H}(\vec{x})\Psi(\vec{x},t), \tag{15}$$

where the state vector $\Psi(\vec{x},t)$ has $2F+1$ components (five in our case), and $\mathcal{H}$ is the Hamiltonian consisting of the kinetic energy term, the bare-atom Hamiltonian and the rf-induced couplings. Equation (15) is then solved for some suitable initial condition $\Psi(\vec{x},0)$.

The true dynamics of evaporative cooling is quite complex, and we can not realistically expect that Eq. (15) describes the situation completely, or that it can be easily solved when all the characteristics of the situation are entered in to the atomic Hamiltonian $\mathcal{H}$. We can, however, make simplifications, some of which have been discussed in the previous section, that nevertheless allow us to convincingly demonstrate some aspects of the rf-induced evaporative cooling, including the nonadiabatic transitions. We restrict our studies to such times that the atoms can re-enter the trap only once. This ignores the possibility of multiple passes, i.e., the possibility that those hot atoms which due to nonadiabatic transitions return to the trap center can reach the rf-resonance again at a later time. For ^{23}Na this approximation is allowed as the rate coefficients for the inelastic processes suggest that only few such atoms can survive until they reach the resonance region again.

Another simplification is that we consider only one spatial dimension, which reduces the situation to the one shown in Fig. 2. However, this is not a crucial simplification. In most cases during the evaporation process the atomic wave packets behave very classically. In this picture only the motion of the atomic wave packet in the direction perpendicular to the rf-induced edge of the trap is needed in studying the nonadiabatic transitions. In other words,

we need to model only that perpendicular motion. Although we allow our wave packets to start from the center of the trap, at the edge of the trap their behavior corresponds also to those atoms that have a more complicated 3D motion but the same behavior in the perpendicular direction near the trap edge. This also means that our approach is valid for all kinds of trap configurations.

For $F = 2$ we get in the bare state basis [from Eqs. (11) and (14)]

$$\mathcal{H} = \begin{pmatrix} T - 2\hbar\sigma(x) & \hbar\Omega & 0 & 0 & 0 \\ \hbar\Omega & T - \hbar\sigma(x) & \sqrt{\frac{3}{2}}\hbar\Omega & 0 & 0 \\ 0 & \sqrt{\frac{3}{2}}\hbar\Omega & T & \sqrt{\frac{3}{2}}\hbar\Omega & 0 \\ 0 & 0 & \sqrt{\frac{3}{2}}\hbar\Omega & T + \hbar\sigma(x) & \hbar\Omega \\ 0 & 0 & 0 & \hbar\Omega & T + 2\hbar\sigma(x) \end{pmatrix} \begin{matrix} |2,-2\rangle_z \\ |2,-1\rangle_z \\ |2,0\rangle_z \\ |2,1\rangle_z \\ |2,2\rangle_z \end{matrix} ; \qquad T = -\frac{\hbar^2}{2m}\frac{\partial^2}{\partial x^2}. \tag{16}$$

We take the mean momentum of the wave packet at the center of the trap as a measure of the kinetic energy of the wave packet. In our study we have selected the radiofrequency such that the crossing of the potentials occurs at the energy corresponding to the kinetic energy of 5 μK in temperature units; see Fig. 2. This sets our bare state trap depth $E_d/k_B = 5$ μK. This is a rather low value, but it is difficult to increase it much more, because the requirements for spatial and temporal step sizes in the numerical treatment of Eq. (15) increase rapidly with E_d. However, we shall later discuss how our results can be scaled into other values of E_d using the multistate Landau-Zener model.

Our trap frequency is 112 Hz, which sets the location of the crossing point at 86 μm from the trap center. The initial wave packet is a Gaussian, which is reasonably narrow in both position and momentum, and moves towards the crossing point. Since the initial kinetic energy in our simulations is of the order of 5 μK, it is possible to obtain narrow distributions in both representations. We distribute the Gaussian wave packet over the bare states so that in fact only the lowest rf-dressed state a is occupied. Similarly, we express the final state populations in terms of the rf-dressed states. However, the five-state problem is easy to define in terms of the bare states, and thus we use this basis for the numerical work. We have propagated the wave packets by splitting the Hamiltonian (16) into a kinetic energy part and a potential energy and coupling part (the split operator method). The kinetic energy part is then treated using the Crank-Nicholson method, and the rest of $\mathcal{H}$ by the diagonalization method. For more details see Ref. [39].

In Fig. 3 we demonstrate how the evaporation works as a function of the kinetic energy $E_{\rm kin}$ of the initial wave packet for different rf-coupling strengths Ω (as defined in Eq. (14)). The curves indicate the probability of the atoms leaving the trap after the first passage of the crossing point by reaching positions $|x| \gg 86$ μm. In addition to showing the total evaporation $P_{\rm evap}$, we also give the contributions (P_a, P_b and P_c) of the individual nontrapped (for $|x| \gg 86$ μm) rf-dressed states a, b and c. Note that $P_{\rm evap} = P_a + P_b + P_c$. For small Ω the evaporation probabilities are clearly peaked at the resonance temperature $E_d = 5$ μK. Also the flat state c dominates the evaporation process, demonstrating nonadiabaticity due to the insufficient coupling strength. However, as Ω is increased, the leading contribution comes from the a state. But although for e.g. $\Omega = (2\pi)$ 3.0 kHz the total evaporation is nearly complete for a large range of temperatures, the contribution from P_b and P_c is still nonnegligible.

Typically one models the level crossings using the Landau-Zener theory, which applies to two-state systems. However, here we have a multistate bowtie crossing model, in which the states are coupled sequentially as in Eq. (14). Fortunately, it has been shown that for the particular case of Eqs. (11) and (14) the bowtie model can be solved analytically [22–24]. In fact, this solution can be expressed in terms of the solutions to the related two-state Landau-Zener (LZ) model, where

$$H_{\rm LZ} = \frac{\hbar}{2}\begin{pmatrix} -\sigma & \Omega \\ \Omega & \sigma \end{pmatrix} \tag{17}$$

According to the five-state case of the model (see e.g. Ref. [24]) the populations for the untrapped states after one traversal of the crossing are

$$\begin{aligned} P_a &= p^4, \\ P_b &= 4(1-p)p^3, \\ P_c &= 6(1-p)^2p^2, \end{aligned} \tag{18}$$

where $p = 1 - \exp(-\pi\Lambda)$ is the probability for adiabatic following in the two-state LZ model of Eq. (17). The adiabaticity parameter Λ is defined for the two-state model as

$$\Lambda = \frac{\hbar\Omega^2}{2\alpha v_C}, \qquad \alpha = \hbar \left.\frac{d\sigma}{dR}\right|_{R=R_C}, \tag{19}$$

where v_C is the speed of the atom at the rf-induced resonance point R_C. It immediately follows that the Landau-Zener model is only applicable when the total energy is higher than the bare-state energy at the resonance point. For more details about applying LZ theory to wave packet dynamics see Refs. [37–39].

For the harmonic trap the atomic mass dependence cancels in Eq. (19), and we obtain

$$\Lambda = 12.0 \frac{1}{F} \frac{[\Omega(\mathrm{kHz})]^2}{\sqrt{E(\mu\mathrm{K}) E_d(\mu\mathrm{K})} [\omega(\mathrm{Hz})]^2} \,, \tag{20}$$

where $E = E_{\mathrm{kin}} - E_d$ and E_{kin} is the kinetic energy of an atom at the trap center. In Fig. 3 we show the LZ predictions as dotted lines together with the actual wave packet results. The agreement is good for $E_{\mathrm{kin}} > 5\mu$K, i.e., when v_C is defined. For smaller kinetic energies the Landau-Zener model cannot be applied, because the model assumes a classical trajectory through the resonance, and for $E_{\mathrm{kin}} < E_d$ this trajectory does not exist.

In Fig. 4 we show the evaporation probability as a function of the initial kinetic energy, expressed in temperature units, for values of Ω large enough that the evaporation is very adiabatic since nearly all atoms leave the trapping region in the rf-dressed state a. The graphs all exhibit a rapid change from trapping into total evaporation around some critical kinetic energy. Since the increase in Ω leads to the lowering of the adiabatic barrier (see Fig. 2) and the atoms follow the rf-dressed states adiabatically, the critical temperature decreases with increasing Ω. However, if we consider the atomic motion in the lowest rf-dressed trapping state classically, we find that the minimum kinetic energy required for total evaporation is larger than the energy required to reach the top of the adiabatic barrier. The top of these barriers is indicated by the plus-signs in Fig. 4. Note that eventually, as E_{kin} increases, the evaporation probability, although not shown here, will again drop.

For many values of the Rabi frequency and kinetic energy the evaporation is not 100 % efficient. Atoms can reflected back into the trap by nonadiabatic transitions in which the atomic wave packet initially on state a encounters the crossing region and is reflected back towards trap center in states a, b or c. The term nonadiabatic is now used in a slightly different fashion to imply that not only the spin state changes, as in the discussion of Fig. 3, but also the direction of the atom has changed. Fig. 5 illustrates for two different values of Ω the probability for returning to the trap center in states a, b, and c. Clearly, if the field is not strong enough, a notable portion of the returning atoms can enter the unwanted b and c states, which correspond to the $(2,1)$ and $(2,0)$ states at the trap center. These nonadiabatic transitions where the atoms return to the trap center are not a direct problem if the collisional loss rates are small enough, since the trapped atoms can be allowed to "slosh" in the trap several times before they exit properly, as discussed by Ketterle and van Druten [14]. However, for ^{23}Na $F = 2$ atoms, these nonadiabatic transitions can cause complications, due to the large inelastic collision rates presented in Sec. II.

Simple estimates can be made for the effect of inelastic collisions due to the hot returning $a = (2,1)$ and $b = (2,0)$ atoms inside the trap. The characteristic time for collisions for rate constant K and density n is $\tau = 1/(Kn)$ and the characteristic mean free path is $x_{\mathrm{mfp}} = 1/(\sigma n) = v/(Kn)$, where σ is the collision cross section and v the relative velocity. With typical condensate densities on the order of 10^{14} atoms/cm^3, τ is on the order of a typical trap vibrational period and x_{mfp} on the order of the trap size for the case of ^{23}Na, whereas τ is much longer than a vibrational period for the case of ^{87}Rb. Therefore, a returning $(2,0)$ ^{23}Na atom is likely to undergo a "bad" inelastic collision that ejects two atoms from the trap, whereas a $(2,0)$ ^{87}Rb atom would pass through the trap unhindered. There could even be problems with collisions in a cold thermal gas above the critical temperature for Bose-Einstein condensation. If nonadiabatic reflection produced $(2,1)$ atoms, they would be trapped, and their density could build up. Near the start of evaporation, where the atoms are still relatively hot, p-wave collisions with $(2,0)$ atoms could result in atom loss, whereas near the end of evaporation where the collision energy is low enough that only s-wave collisions are significant, a build up of $(2,1)$ population would result in losses due to collisions between $(2,1)$ atoms with a time constant determined by the $(2,1)$ density. This could easily be less than 1 s for ^{23}Na even if only a small fraction of the $(2,2)$ population were converted to $(2,1)$. These considerations suggest that evaporative cooling of ^{23}Na in the $(2,2)$ state may be much more difficult than for ^{87}Rb, for which evaporative cooling is known to work [1]. The rf power in the ^{23}Na case would have to be sufficiently high to avoid nonadiabatic trap dynamics.

The multistate Landau-Zener model cannot describe the sequence of classical trajectories that leads to nonadiabatic reflection back into the center of the trap. This setback is not very important, because it is clear that if the evaporation process is effective for a single pass, then necessarily we can ignore any nonadiabatic effects. Since our wave packet results show that the multistate Landau-Zener theory is a good model for evaporation without reflection, we can always determine for any temperature and trap frequency the minimum rf-field strength that is required to quench the nonadiabatic processes by making the single-pass evaporation nearly 100 % effective. This is achieved by requiring that $\Lambda \gg 1$ in Eq. (20).

IV. CONCLUSIONS

We have shown that in the ^{23}Na $F = 2$ system inelastic low-temperature collision rate coefficients can be larger than 10^{-11} cm^3/s. These rate coefficients occur when the collision partners are (2,1) and (2,1), or (2,2) and (2,0). For ^{87}Rb we find that all rate coefficients are small, on the order of 10^{-14} cm^3/s. Another interesting outcome of our studies is the fact that rf-induced mixing plays no role in the occurrence of the inelastic processes. The rf-dressed states are obtained from the bare states by a rotation. However, this basis change does not alter the physics of the situation, it merely redefines the quantization axis for the atomic angular momentum.

In the absence of any mixing effects the inelastic processes in the ^{23}Na $F = 2$ system can occur only if we have true occupation of the rf-dressed states labelled as $(2, 1)$ or $(2, 0)$. Such occupation can be created by nonadiabatic population transfer from the $(2, 2)$ rf-dressed state to the other rf-dressed states. As the atoms move in spatially inhomogeneous fields, the local orientation of the quantization axis (B-field) may change faster than the ability of the system to follow it adiabatically. With wave packet simulations we have demonstrated that the rf-field can induce such nonadiabatic transfer during evaporative cooling. Furthermore, it is clear that due to this transfer atoms can return to the trap center while occupying the rf-dressed states $(2, 1)$ and $(2, 0)$.

The above effect can be reduced by keeping the strength of the rf-field so large that the adiabatic following is ensured. However, at the early stages of evaporative cooling the spatial change of potentials near the field-induced resonance can be rapid. This can make it rather difficult to achieve the total adiabatic following. In addition the p-wave contributions to the inelastic processes are nonnegligible when $T \gtrsim 100$ μK (for ^{23}Na). Under these circumstances one can not allow the hot atoms to slosh in the trap too much before they leave it. So far condensation has not been demonstrated for the ^{23}Na $F = 2$ system. We believe that, in order to achieve it, one has to use clearly stronger rf-fields than e.g. for the ^{23}Na $F = 1$ system.

Our simulations have also demonstrated that the multistate Landau-Zener model [22–24] can predict the basic wave packet dynamics of the evaporation process correctly. This multistate model can be given a simple analytic solution only when we have equal energy differences between subsequent states and the sequential couplings given in Eq. (14). If the rf-dressing of the states could not be described by the simple rotation of the quantization axis, then the solution of the model would have to include the complicated construction of the continuously changing dressed states from the bare states, in addition to the actual nonadiabatic processes. This is clearly connected to the fact that a simple solution for the multistate LZ model in terms of the two-state case exists only for this particular case. Despite its limitations, however, the multistate LZ model gives us a simple and reliable criterion for making evaporation so efficient that nonadiabatic transitions are strongly quenched.

Recently it was shown experimentally that a ^{87}Rb $(1, -1)$ condensate can be converted into a $(2, 1)$ condensate with a microwave pulse [40]. Our results for ^{23}Na $(2, 1)$+$(2, 1)$ collisions suggest that a similar experiment with the ^{23}Na system would not work. However, such an experiment might be used to verify the loss rates presented in this paper, as the pulsed creation of a $(2, 1)$ condensate allows one to set a distinctive time point for the beginning of its destruction.

In addition to the process illustrated in Sec. III nonadiabatic transfer can also arise if the frequency of the rf-field is not changed slowly compared to the other time scales of the system. The moving atoms would then see a chirped field, and the speed v_C in the Landau-Zener model would correspond more to the change of location of the rf-resonance point, than to the actual atomic wave packet motion through the resonance. This chirped rf-field case could be studied with wave packet dynamics [41]. It is also used in the output coupler schemes for the trapped condensates [10]. However, we have assumed that the rf-field frequency ν is changed so slowly that this effect does not arise.

A similar situation, i.e., motion of the crossing point past the atoms, can occur in the TOP trap, as discussed in Sec. II [35]. It is generally assumed that the TOP field changes so fast that the passing of the resonance is completely diabatic—this also means that the rf-field can be ignored when the time-averaged field is determined for the TOP trap. If the passing of the resonance were strongly adiabatic, the time-average would have to be performed *after* adding the rf-induced resonances and couplings. Then very interesting effects might arise (for an example see Ref. [42]).

ACKNOWLEDGMENTS

This research has been supported by Army Research Office, Office for Naval Research and the Academy of Finland.

* Current address: Department of Chemistry and Biochemistry, University of Maryland, College Park, MD 20742.

[1] M. H. Anderson, J. R. Ensher, M. R. Matthews, C. E. Wieman, and E. A. Cornell, Science **269**, 198 (1995).
[2] K. B. Davis, M.-O. Mewes, M. R. Andrews, N. J. van Druten, D. S. Durfee, D. M. Kurn, and W. Ketterle, Phys. Rev. Lett. **75**, 3969 (1995).
[3] M.-O. Mewes, M. R. Andrews, N. J. van Druten, D. M. Kurn, D. S. Durfee, and W. Ketterle, Phys. Rev. Lett. **77**, 416 (1996).
[4] C. C. Bradley, C. A. Sackett, and R. G. Hulet, Phys. Rev. Lett. **78**, 985 (1997).
[5] D. S. Jin, J. R. Ensher, M. R. Matthews, C. E. Wieman, and E. A. Cornell, Phys. Rev. Lett. **77**, 420 (1996).
[6] M. Edwards, P. A. Ruprecht, K. Burnett, R. J. Dodd, and C. W. Clark, Phys. Rev. Lett. **77**, 1671 (1996).
[7] M.-O. Mewes, M. R. Andrews, N. J. van Druten, D. M. Kurn, D. S. Durfee, C. G. Townsend, and W. Ketterle, Phys. Rev. Lett. **77**, 988 (1996).
[8] D. S. Jin, M. R. Matthews, J. R. Ensher, C. E. Wieman, and E. A. Cornell, Phys. Rev. Lett. **79**, 764 (1997).
[9] M. R. Andrews, D. M. Kurn, H.-J. Miesner, D. S. Durfee, C. G. Townsend, S. Inouye, and W. Ketterle, Phys. Rev. Lett. **79**, 553 (1997).
[10] M.-O. Mewes, M. R. Andrews, D. M. Kurn, D. S. Durfee, C. G. Townsend, and W. Ketterle, Phys. Rev. Lett. **78**, 582 (1997).
[11] M. R. Andrews, C. G. Townsend, H.-J. Miesner, D. S. Durfee, D. M. Kurn, and W. Ketterle, Science **275**, 637 (1997).
[12] H. F. Hess, Phys. Rev. A **34**, 3476 (1986).
[13] T. Tommila, Europhys. Lett. **2**, 789 (1986).
[14] W. Ketterle and N. J. van Druten, Adv. At. Mol. Opt. Phys. **37**, 181 (1996).
[15] D. E. Pritchard, K. Helmerson, and A. G. Martin, At. Phys. **11**, 179 (1988).
[16] H. T. C. Stoof, A. M. L. Janssen, J. M. V. A. Koelman, and B. J. Verhaar, Phys. Rev. A **39**, 3157 (1989).
[17] E. Tiesinga, S. J. M. Kuppens, B. J. Verhaar, and H. T. C. Stoof, Phys. Rev. A **43**, R5188 (1991).
[18] F. H. Mies, C. J. Williams, P. S. Julienne, and M. Krauss, J. Res. Nat. Inst. Stand. Technol. **101**, 521 (1996).
[19] S. J. J. M. F. Kokkelmans, H. M. J. M. Boesten, and B. J. Verhaar, Phys. Rev. A **55**, R1589 (1997).
[20] P. S. Julienne, F. H. Mies, E. Tiesinga, and C. J. Williams, Phys. Rev. Lett. **78**, 1880 (1997).
[21] Here "bare" states are atom-field product states with energy equal to that for the atom and the field before taking into account the atom-field interaction, and "dressed" states are those which result from diagonalizing the Hamiltonian including the atom-field interaction.
[22] A. K. Kazansky and V. N. Ostrovsky, J. Phys. B **29**, L855 (1996).
[23] V. N. Ostrovsky and H. Nakamura, J. Phys. A **30**, 6939 (1997).
[24] N. V. Vitanov and K.-A. Suominen, Phys. Rev. A **56**, R4377 (1997).
[25] A. J. Moerdijk, B. J. Verhaar, and T. M. Nagtegaal, Phys. Rev. A **53**, 4343 (1996).
[26] H. T. C. Stoof, J. M. V. A. Koelman, and B. J. Verhaar, Phys. Rev. B **38**, 4688 (1988).
[27] C. J. Myatt, E. A. Burt, R. W. Ghrist, E. A. Cornell, and C. E. Wieman, Phys. Rev. Lett. **78**, 586 (1997).
[28] F. H. Mies, Phys. Rev. A **7**, 942 (1973).
[29] W. E. Baylis, J. Pascale, and F. Rossi, Phys. Rev. A **36**, 4212 (1987).
[30] C. J. Williams, F. H. Mies, and P. S. Julienne, unpublished.
[31] E. Tiesinga, C. J. Williams, P. S. Julienne, K. M. Jones, P. D. Lett, and W. D. Phillips, J. Res. Nat. Inst. Stand. Technol. **101**, 505 (1996).
[32] S. Inouye, M. R. Andrews, J. Stenger, H.-J. Miesner, D. M. Stamper-Kurn, and W. Ketterle, Nature **392**, 151 (1998).
[33] J. P. Burke Jr, J. L. Bohn, B. D. Esry, and C. H. Greene, Phys. Rev. A **55**, R2511 (1997).
[34] J. Vanier and C. Audoin, *The Quantum Physics of Atomic Frequency Standards* (Adam Hilger, Bristol, 1989).
[35] K. Helmerson and W. D. Phillips, private communication.
[36] R. N. Zare, *Angular momentum* (Wiley, New York, 1988).
[37] K.-A. Suominen and B. M. Garraway, Phys. Rev. A **48**, 3811 (1993).
[38] K.-A. Suominen, M. J. Holland, K. Burnett, and P. S. Julienne, Phys. Rev. A **49**, 3897 (1994).
[39] B. M. Garraway and K.-A. Suominen, Rep. Prog. Phys. **58**, 365 (1995).
[40] M. R. Matthews, D. S. Hall, D. S. Jin, J. R. Ensher, C. E. Wieman, and E. A. Cornell, preprint LANL cond-mat/9803310 (1998); D. S. Hall, M. R. Matthews, J. R. Ensher, C. E. Wieman, and E. A. Cornell, preprint LANL cond-mat/9804138 (1998).
[41] A. Paloviita, K.-A. Suominen, and S. Stenholm, J. Phys. B **28**, 1463 (1995); A. Paloviita, Opt. Commun. **119**, 533 (1995).
[42] R. Dum, A. Sanpera, K.-A. Suominen, M. Brewczyk, M. Kuś, K. Rzążewski, and M. Lewenstein, Phys. Rev. Lett. **80**, 3899 (1998).

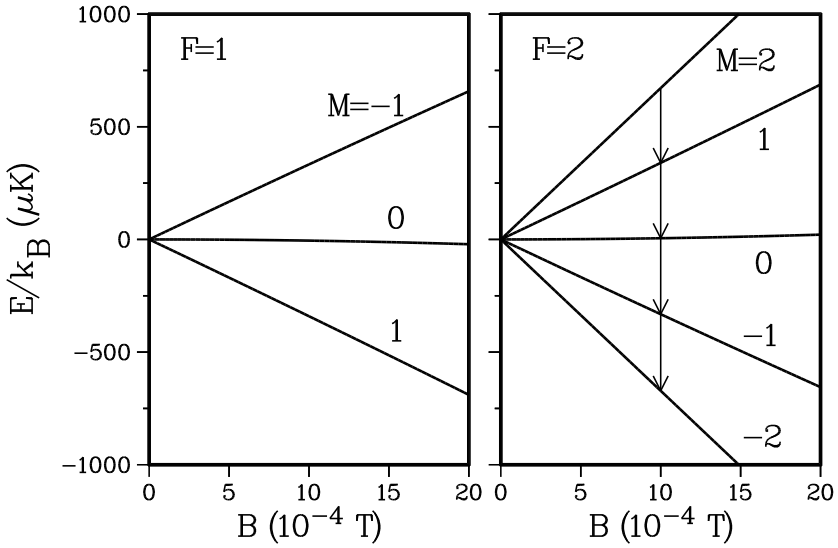

FIG. 1. The hyperfine structure of the ground state for ^{23}Na as a function of magnetic field B. In a typical trapping situation the $F = 1$, $M = -1$ or $F = 2$, $M = 2$ state is used, B depends quadratically on a spatial coordinate and is on the order of 1 mT in the middle of the trap. The left frame shows the magnetic field dependence of the three $F = 1$ magnetic sublevels. For fields up to 2 mT the internal energy is in the linear Zeeman regime. The right frame shows the five $F = 2$ sublevels. The arrows indicate the rf-induced coupling between the various sublevels for an atom initially in the $F = 2$, $M = 2$ state, where the length of the arrow is proportional to the rf frequency ν.

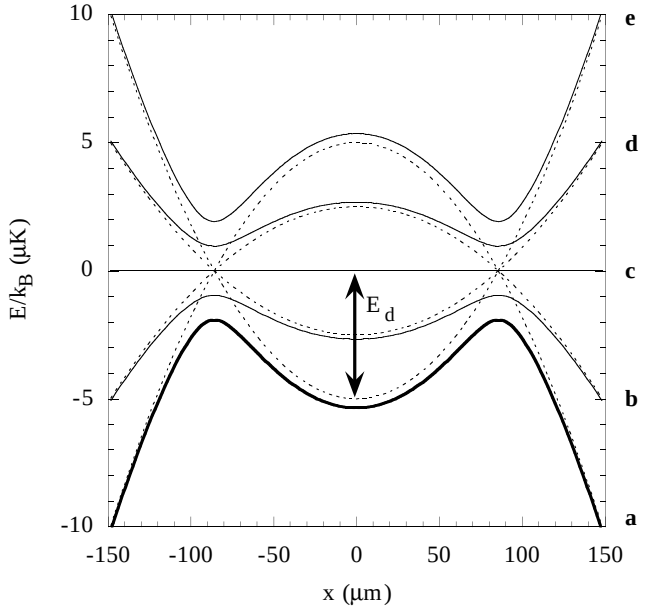

FIG. 2. Bare potentials (dotted lines) and corresponding rf-dressed potentials (solid lines) for the ^{23}Na $F = 2$ system. After performing the rotating wave approximation the atomic states are shifted by multiples of the rf-field quantum and rf-resonances occur as crossings. The trap frequency is 112 Hz. The bare state trap depth is $E_d/k_B = 5$ μK. The rf-field is resonant with the M-states at $x \simeq 86$ μm. The bare potentials are at the center of the trap $M = 2, 1, 0, -1, -2$, in the order of increasing energy. Correspondingly the rf-dressed states are labelled from a to e. The trapping state a is indicated by a thick solid line.

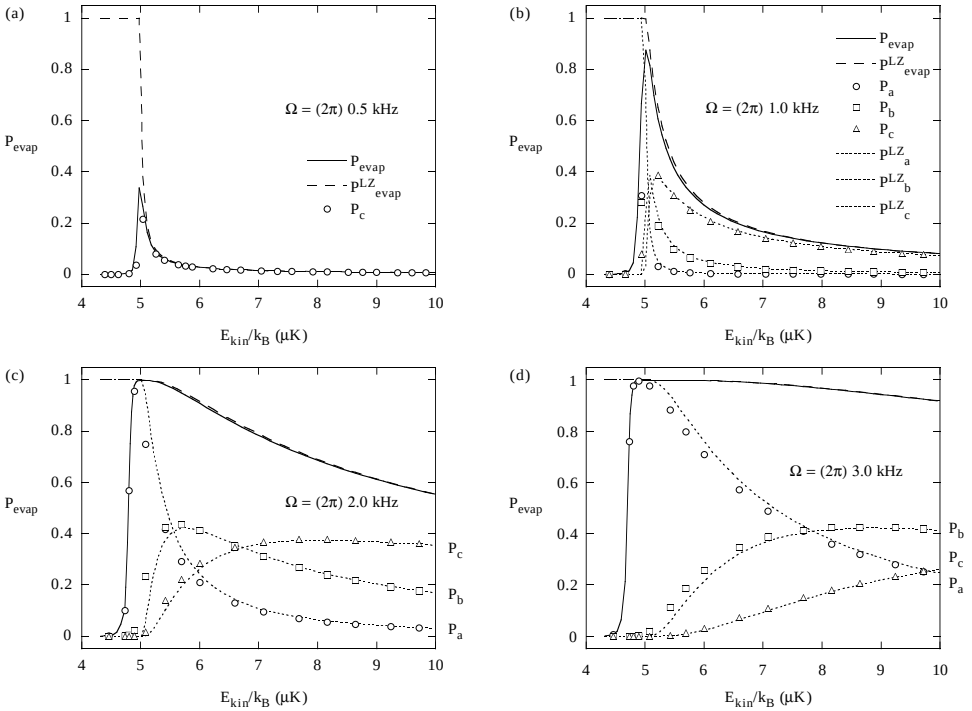

FIG. 3. The evaporation probability $P_{\rm evap}$ as a function of the initial kinetic energy of the Gaussian wave packet for a selection of Rabi frequencies after a single passage through the rf-induced resonance. We show the wave packet results for total evaporation (solid line), and the individual rf-dressed state contributions P_a, P_b and P_c when they are nonnegligible. The dotted lines give the predictions by the multistate Landau-Zener model for the probability of escaping the trap for the rf-dressed states a, b and c. The dashed lines, labeled $P_{\rm evap}^{\rm LZ}$, represent the total evaporation probability given by the multistate Landau-Zener model.

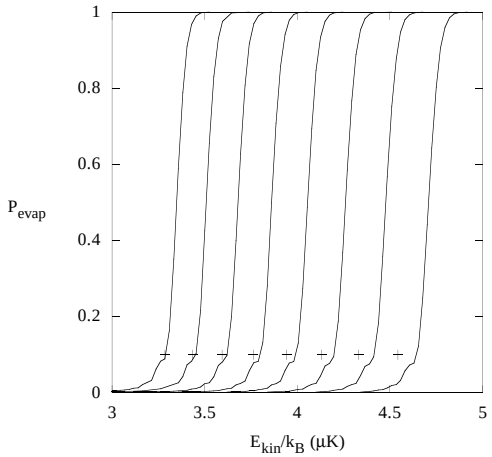

FIG. 4. The wave packet results for the total evaporation probability $P_{\rm evap}$ as a function of the initial kinetic energy. The values of the coupling $\Omega/(2\pi)$ are from right to left: $2.5, 5, 7.5, 10, 12.5, 15, 17.5, 20$ kHz. The plus-signs mark the corresponding energy values where the barrier height for the rf-dressed states is located in energy.

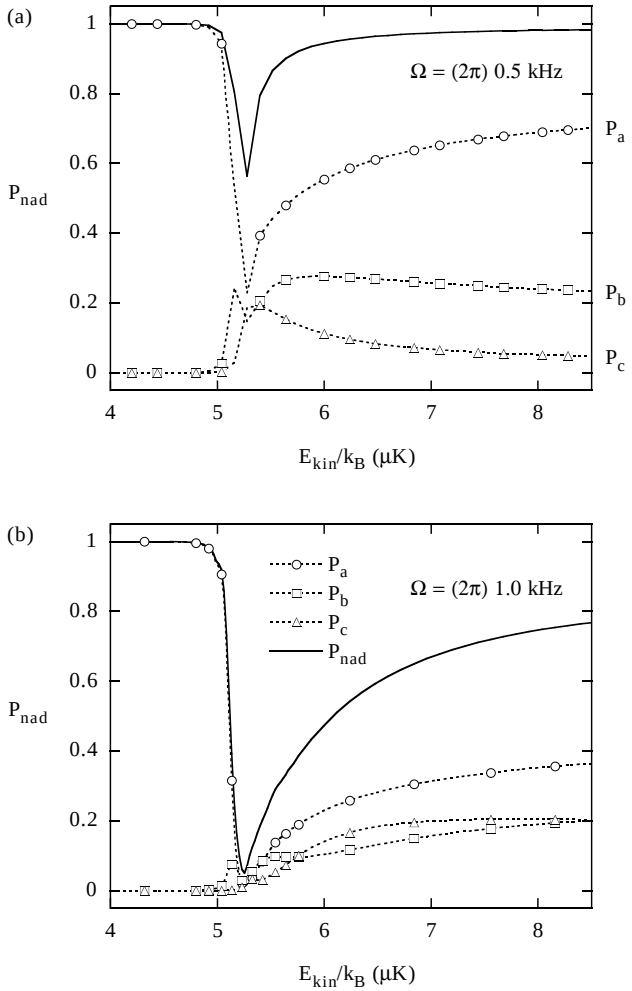

FIG. 5. The nonadiabatically induced population $P_{\rm nad}$ of the three lowest rf-dressed states (a, b and c) after a reflection from the rf-resonance point as a function of the initial kinetic energy. The solid line indicates the summed population of the three states.